Desalination and Water Treatment
www.deswater.com

doi: 10.5004/dwt.2020.26186

202 (2020) 364–380
October

Preparation and characterization of a recyclable high-branched/generation dendrimer nano-polymer based on the enhanced magnetic core for naphthalene sorption from aqueous solutions

Shahrzad Aliannejadi[a], Amir Hessam Hassani[a], Homayon Ahmad Panahi[b,*], Seyed Mehdi Borghei[c]

[a]*Department of Environmental Engineering, Faculty of Natural Resources and Environment, Science and Research Branch, Islamic Azad University, Tehran, Iran, emails: sh.aliannejad@gmail.com (S. Aliannejadi), ahhassani@srbiau.ac.ir (A.H. Hassani)*
[b]*Department of Chemistry, Central Tehran Branch, Islamic Azad University, Tehran, Iran, Tel. +982144164539; Fax: +982144164539; email: h.ahmadpanahi@iauctb.ac.ir (H.A. Panahi)*
[c]*Department of Chemical and Petroleum Engineering, Sharif University of Technology, Tehran, Iran, email: mborghei@sharif.edu (S.M. Borghei)*

Received 15 November 2019; Accepted 1 June 2020

ABSTRACT

In this study, silica-coated magnetic nanoparticles (SCMNPs) were modified with ten generations of organic dendrimer containing methyl acrylate and melamine. At the final stage, benzophenone ligand bonded as an active surface actuator functional group on the sorbent product. This novel nanosorbent was used for naphthalene (NAP) removal. The synthesized nanosorbent was characterized by X-ray diffraction, thermogravimetric analysis, Fourier-transform infrared spectroscopy, vibrating sample magnetometry, Brunauer–Emmett–Teller, and scanning electron microscopy–energy-dispersive X-ray spectroscopy. The diameter range of the final sorbent was found 20–70 nm. The operational sorption parameters were optimized in a batch system. The best removal efficiency was obtained at pH = 7 during a 20 min process with the 0.4 g L^{-1} sorbent dosage in the presence of 20 mg L^{-1} NAP at 25°C. Finally, NAP removal from the real samples (complex industrial waste and aqueous samples) was studied via gas chromatography-mass spectrometry with the 90%–100% NAP removal from the samples. The data were evaluated with various isotherm models and kinetic studies where the Langmuir isotherm exhibited a high compatibility (R^2 = 0.9969) in the pseudo-second-order kinetic (R^2 = 0.9998) process. The present study revealed that the synthesized magnetic polymer has a high protentional for NAP removal from aqueous samples (>99%), because of the high sorption capacity (q_m = 94.33 mg g^{-1}), pH independence, rapid sorption process, and high recovery.

Keywords: High branched dendrimers; Naphthalene sorption; Industrial wastewater; Modified magnetic nanoparticles; Reusability

1. Introduction

Polycyclic aromatic hydrocarbons (PAHs) are an essential class of oil contaminants containing two or several aromatic rings with carbon and hydrogen atoms [1]. Oil and petrochemical waste, incomplete combustion of organic compounds, firing in fields, and leakage from storage tanks are among the sources for releasing these compounds into the environment [2]. PAHs are hydrophobic chemical groups of compounds with high stability in the environment and high penetration in the soil and water. PAHs have a low solubility in water with a high boiling/melting point [3,4]. High toxicity, the hazardous effect on the health of individuals, teratogenic defects, and carcinogenetic/mutagenic features are among

* Corresponding author.

their other properties [4,5]. Accordingly, the Environmental Protection Agency (EPA) regards PAHs as pollutant compounds with high priority [1]. Thus, the presence of these compounds in the environment is a high-risk issue, and they must be removed from aqueous media [6].

Among the different strategies for PAHs removal, adsorption techniques are common as they are efficient and simple to use [7,8]. Nanoparticles, especially magnetic nanoparticles (MNPs), have been introduced to many applications as they enjoy a high surface to volume ratio, non-toxicity, rapid adsorption, super magnetic properties, are environmentally friendly, and can be easily separated from solutions through an external magnetic field [9]. Different studies have reported the application of MNPs for the removal of environmental pollutants such as dyes, [10] metals, and chemicals [11]. MNPs can be prepared through different methods such as hydrothermal, co-precipitation, thermal decomposition, and microemulsion method [12]. The co-precipitation method is a simple technique with high performance in producing homogeneous particles on a small scale [13]. Silica, as a covering-protecting layer for MNPs, which prevents rapid oxidation, particle accumulation and morphological changes, can be used to provide active sites for surface modification and bonding with polymer molecules through modifying functional groups at the surface [14].

Dendrimers are high-branched synthetic polymers on the nanoscale with three-dimensional spherical structures arranged orderly. These symmetric-mono dispersed macromolecules contain a central core, as well as repetitive groups from the core in the branch configuration, which end in the terminal groups after several generations [15,16]. Dendrimer generations form from the successive repetition of branches. The reactivity, as well as the stability of dendrimers, can be determined based on the terminal ligand nature [17] modifiability of the branch structure and internal/external groups, high density, controlling the generation number, and changing the chemical/physical properties are among the other benefits for the dendrimers [8,15,18]. Thus, they are used in different scientific fields and industrial areas. Unique properties including numerous internal sites among the branches to encapsulate guest molecules, designing capability of terminal groups concerning target pollutants, and increasing the sorption capacity make them ideal a sorbent in the water purification technique [16,19]. Many studies have reported the removal of pollutants and purification of aqueous solutions using dendrimers [20,21]. However, there are few studies on PAHs removal using dendrimeric sorbents such as pyrene [22] as well as the elimination of polyaromatic compounds [8] from aqueous environments.

The aim of this research is to fabricate, modify, and apply a novel nanosorbent with high recovery and sorption capacity for naphthalene (NAP) adsorption from wastewater and to evaluate the operating parameters in the adsorption process. The final magnetic dendrimer was synthesized to enhance the sorption capacity through continuous polymerization and controlled ten-generation on the magnetic core of iron-oxide. The high-branched nanosorbent included ligands containing terminal benzene rings in dendrimer structures bonding to the dendrimer polymer chain through covalence bonding. The π-benzophenone mutual effects and numerous internal sites enhance the intermolecular interactions to boost the adsorption of non-saturated and non-polar organic molecules (i.e., PAHs, NAP). The synthesized nanostructures were characterized by X-ray diffraction (XRD), thermogravimetric analysis (TGA), vibrating sample magnetometry (VSM), Fourier-transform infrared spectroscopy (FTIR), scanning electron microscopy–energy-dispersive X-ray spectroscopy (SEM-EDS) analyses. Further, operating parameters such as sorbent dosage, pH, temperature, NAP concentration, and contact time were examined the sorption process. Also, the sorbent recovery, isotherms models, and kinetic studies were evaluated. The gas chromatography-mass spectrometry (GC-MS) analysis was conducted to extract naphthalene from the wastewater and surface water as real samples.

2. Experimental setup

2.1. Materials

$FeCl_2{\cdot}4H_2O$, $FeCl_3{\cdot}6H_2O$, (3-aminopropyl)triethoxysilane (APTES), tetraethyl orthosilicate, dried toluene, methanol, methyl acrylate (MA), 2,4,6-triamino-1,3,5-triazine with the industrial name melamine (MEL), benzophenone (BF), 25% ammonia solution, ethanol, naphthalene (NAP), phosphoric acid, boric acid, sodium hydroxide, and acetic acid were used in the high purity, (assay > 95%) provided by Merck (Darmstadt, Germany).

2.2. Instruments

XRD analysis was used to determine the crystal structure and the crystal phase of the nanosorbent with the Cu-Kα irradiation λ = 1.5406 Å within the angle range of 2θ = 10–80 (PANalytical, England). To determine the functional groups and bonds, FTIR (410, Jasco Inc., Easton, Maryland, USA) was used. TGA was employed via TGA (Rheometric Scientific, STA 1500 model, Switzerland) within the temperature range of 0°C–600°C in the air atmosphere at 10°C min^{-1}. SEM (TE-SCAN, Czechoslovakia) equipped with energy-dispersive X-ray spectroscopy (EDS) was applied to obtain the morphology and size of the nanoparticles as well as for elemental analysis of the samples. The magnetic properties of the samples were investigated by VSM (LBKFB model, Meghnatis Kavir, Iran). The Brunauer–Emmett–Teller (BET) surface area was determined via N_2 adsorption/desorption isotherm using a Quantachrome NOVA 2200E system (Austria). The pore volume and pore size were calculated using the Barrett–Joyner–Halenda (BJH). Pollutant concentrations were evaluated by a UV-Vis spectrophotometer (Perkin Elmer, Lambda25, USA). To extract naphthalene from real wastewater samples and aqueous solutions, GC-MS (GC 7890N equipped with MS 5975C, Model EI Agilent, USA) was conducted.

2.3. Preparation of MNPs covered by SiO_2

Fe_3O_4 nanostructures were synthesized by the co-precipitation method [23,24]. Initially, a homogeneous mixture of 0.994 g $FeCl_2$ and 2.7 g $FeCl_3$ salts (2:1 molar ratio)

was prepared in 100 mL deionized water without O_2 gas. By adding an ammonia solution (25%) dropwise, the color of the mixture changed from orange to black (pH = 10–11). The mixing continued for 2 h in a paraffin bath at 80°C and N_2 atmosphere. Once cooled down to room temperature, the black precipitates were collected using an external magnet [25,26]. The resulting particles were MNPs (Fe_3O_4). Silica coating was then added to the Fe_3O_4. To do this, the synthesized Fe_3O_4 was mixed with ethanol and tetraethyl orthosilicate (80 and 40 mL respectively), at room temperature and stirred for 24 h. The nano core-shell particles were separated by an external magnet and washed several times with DI water and ethanol. The resulting particles were silica-coated magnetic nanoparticles (SCMNPs), which were dried in a vacuum oven at 40°C [23,27].

2.4. Adding APTES to SCMNPs

About 47.5 mL dried toluene and 2.5 mL APTES were mixed in a round-bottom flask, to which and 1.5 g of SCMNPs prepared in the previous step was added. The mixture was refluxed at 80°C for 48 h. The precipitates were collected by a magnet and washed with toluene and dried at a vacuum oven at 40°C [23,26].

2.5. Grafting of MA/MEL polymer dendrimers on modified MNPs

To synthesize the dendrimer branches and polymer generations using the divergent method, we used two additional reactions of MA and MEL continuously. Initially, 15 mL MA was mixed with 150 mL methanol mixed in a two-neck rounded bottom flask and the synthesized SCMNPs/APTES was added to it. The mixture was stirred at 50°C for 24 h in reflux conditions under N_2. The final powder was collected by a magnet. In this way, the half-generation dendrimer product was prepared (MA/MEL-DG-0.5).

Specifically, 150 mL ethanol and 1 g MEL were added to the above product and refluxed in a water bath under N_2 at 80°C for 8 h. The final product was separated by a magnet (MA/MEL-DG-1). By repeating the same steps of these two reactions, a greater generation of dendrimer was achieved, which was continued up to the ten-generation in this work (MA/MEL-DG-10) [20,28].

2.6. Modification of SCMNPs/APTES@(MA/MEL-DG-10) with benzophenone ligand

About 150 mL methanol was mixed with 1 g BF in a 250 mL flask and later added to the prepared magnetic dendrimers under N_2 in reflux condition for 6 h at 50°C waterbath. The final synthesized nanostructures were washed with ethanol and dried at a vacuum oven.

The synthesis method of the modified magnetic dendrimer product and NAP adsorption mechanism is illustrated in Figs. 1 and 2 respectively.

2.7. Study method

Bach system and synthetic solutions were used in this study. At first, 100 mg L^{-1} NAP stock solution was prepared in water/ethanol (30% v/v) which was later used for preparing other concentrations of solutions. To obtain the best sorption efficiency of NAP from the aqueous solutions via the synthetic nanopolymer product, operating parameters in the adsorption process including pH (3–10), contact time (2–90 min), temperature (15°C–45°C), sorbet dosage (0.01–2 g L^{-1}), and initial NAP concentration (1–80 mg L^{-1}) were investigated. All the experiments were performed by alternating one parameter once while keeping the other factors constant. To adjust the pH of the NAP sample solutions, buffer solutions (pH = 3–10) containing 0.05 M acetic acid, 2.0 M sodium hydroxide, 0.04 M boric acid, and 0.06 M phosphoric acid were used. The initial and residual concentrations of NAP were read at λ_{max} = 276 nm via UV-Vis spectroscopy. Finally, the optimized parameters for SCMNPs/APTES@(MA/MEL)DG-10/BF sorbent products in the process were used to remove NAP from real aqueous solutions. To this end, NAP removal content was measured via the GC-MS technique from industrial waste, seawater, and river water. Each experiment was repeated three times for the real samples.

Freundlich, Redlich–Peterson, Langmuir, and Temkin models were used to analyze the adsorption mechanism. To determine the isotherm models, NAP solutions (1–50 mg L^{-1}) were prepared with 0.4 g L^{-1} sorbent product at pH = 7. The mixtures were shaken for about 20 min at 150 rpm. Then, the mixtures were centrifuged at 5,000 rpm for 5 min with the supernatant read by a UV-Vis spectrophotometer. In this work, three kinetic models, including pseudo-first-order, pseudo-second-order, and intraparticle diffusion, were evaluated. Kinetic studies were conducted within 2–90 min contact time, with 20 mg L^{-1} NAP at 150 rpm at pH = 7 in the presence of 0.4 g L^{-1} sorbent product. The naphthalene removal [Eq. (1)] and sorption capacity [Eq. (2)] of the synthetic nanopolymer were obtained from the following equations [4,23,29]:

$$R_E = \frac{\left(C_0 - C_e\right)}{C_0} \times 100 \tag{1}$$

$$q_e = \frac{\left(C_0 - C_e\right) \times V}{W} \tag{2}$$

where R_E (%) is removal efficiency, C_0 (mg L^{-1}) denotes the initial concentration of pollutant, C_e (mg L^{-1}) shows the pollutant concentration at the equilibrium, q_e (mg g^{-1}) denotes the pollutant adsorbed per sorbent weight, V(L) shows the volume of the solution, and W(g) is the sorbent weight.

2.8. Determination of point of zero charge (pH_{pzc})

pH_{PZC} is the point at which the surface charge of the adsorbent is neutral. To investigate the pH of the point of zero charge (pH_{PZC}), first, 0.01 M NaCl solution (25 ml volume) was poured in eight beakers. Their pH was measured by a pH-meter apparatus. Then, 0.1 M HCl and sodium hydroxide solutions were used for adjusting the pH at 3 to 10. The adsorbent was then added to each beaker at the concentration of 0.2 g L^{-1}. The samples were mixed on a shaker for 24 h. The pH of the solutions was then measured again by the pH-meter apparatus.

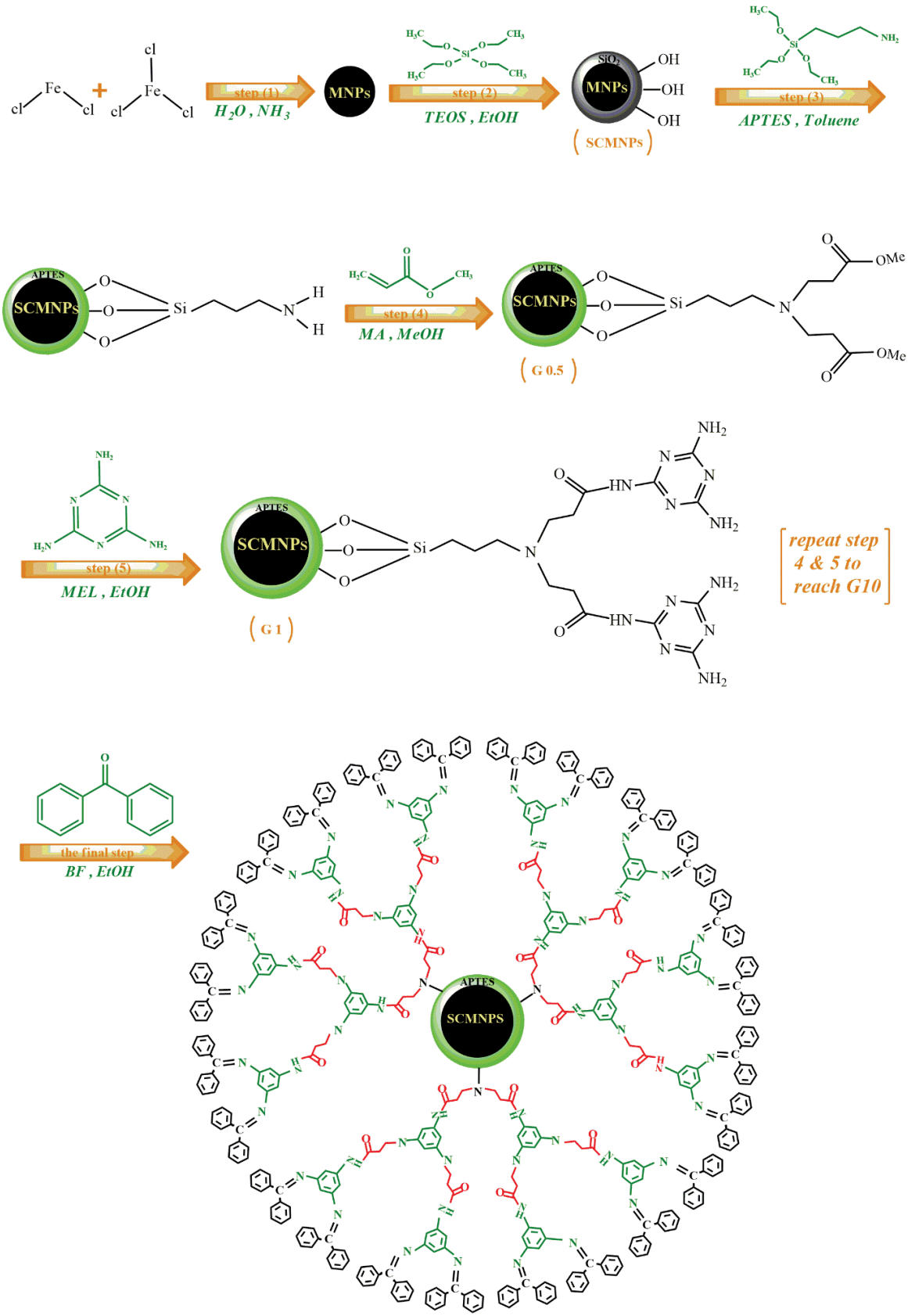

Fig. 1. Preparation and modification of SCMNPs/APTES@(MA/MEL)DG-10/BF.

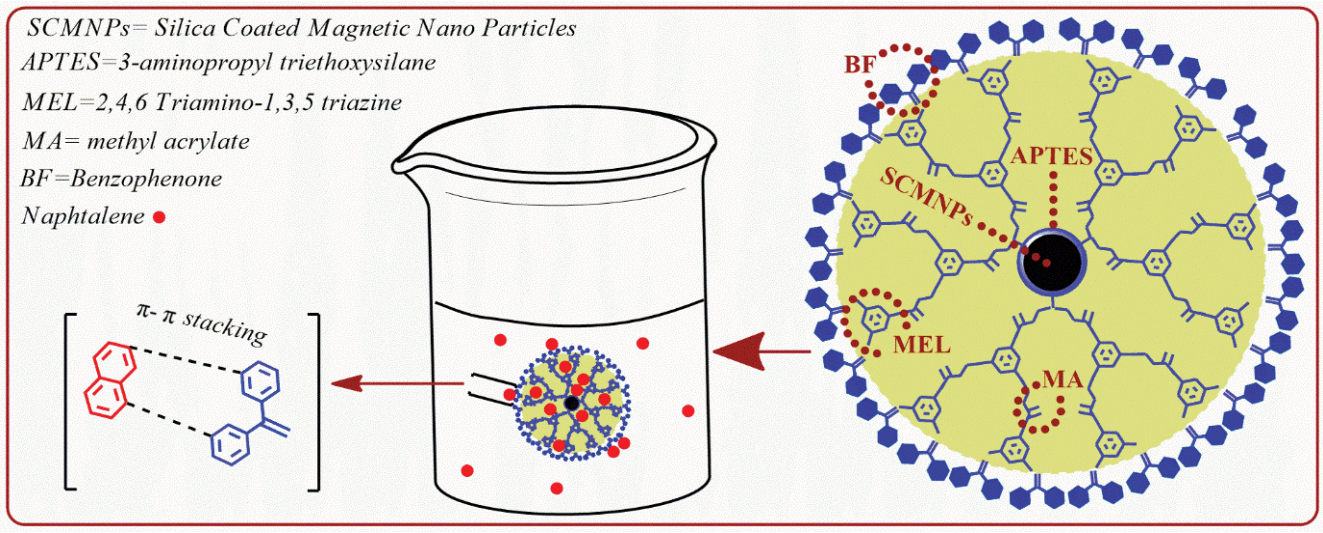

Fig. 2. NAP adsorption mechanism onto the synthesized magnetic dendrimer.

2.9. Recovery and reusability of SCMNPs/APTES@(MA/MEL) DG-10/B nanopolymer

Reusability and recovery of the sorbent are critical issues in water purification technologies and are important in many industrial applications. The quantitative desorption of NAP from the synthesized sorbent was studied using several eluents (ethanol, methanol, and acetone). It was found that ethanol was sufficient for the desorption of NAP (>90%) from the sorbent [30]. The solubility of NAP is higher in ethanol and a higher desorption rate can be achieved with lower ethanol consumption when compared to the other two substances. In order to estimate the reusability of SCMNPs/APTES@(MA/MEL)DG-10/B adsorbent, the adsorption–desorption cycle was repeated ten times under optimal conditions. Based on the results of sorption studies, optimum values were used in the experiments (pH 7, contact time 20 min, 0.4 g L^{-1} sorbent dosage, 20 mg L^{-1} NAP at 25°C). In each cycle for recovery and separate the targeted pollutant from the sorbent, 10 mL of ethanol was used. The sorbent and ethanol mixture was shaken for 15 min at 50°C and then sonicated for 10 min. The adsorption–desorption cycle procedure was repeated ten times using the same adsorbent, and the removal efficiency reported for every cycle.

2.10. Comparison of the NAP removal percentage by magnetic nanosorbents prepared in different steps of this study

In this step, five flasks containing 25 mL of 20 mg L^{-1} NAP solution were prepared to which 0.01 g of the sorbent products including SCMNPs, SCMNPs/APTES, SCMNPs/APTES@(MA/MEL)DG-5, SCMNPs/APTES@(MA/MEL)DG-10 and SCMNPs/APTES@(MA/MEL)DG-10/BF were added (sorbent dosage 0.4 g L^{-1}). The mixtures were shaken for 15 min. All the experiments were conducted based on the obtained optimized parameters. The mixtures were centrifuged, with the NAP concentration in the solution determined by a UV-Vis spectrophotometer.

2.11. GC-MS procedure

To evaluate the adsorption of SCMNPs/APTES@(MA/MEL)DG-10/BF for NAP removal from aqueous samples, real samples were also studied alongside the adsorption experiments of synthetic samples. To this aim, samples were taken from industrial waste, seawater, and river water all containing NAP. Qualitative and quantification analyses were conducted by the GC-MS method. The system was equipped with an MS detector and capillary column (30 m) with an inner diameter of 0.25 mm and 0.25 μm thickness in the HP5-MS phase. The inlet temperature was set to 290°C and helium was used as carrier gas with a flow rate of 1 mL min^{-1}. The sample volume was 1 μL with a split ratio of 5:1. The initial temperature for the oven was 110°C and kept for 5 min. The temperature rate was set to 5°C/min up to 290°C and was kept for 10 min at this temperature.

NAP content was measured in the samples (before and after the sorption process) via GC-MS. Also, 2, 5, and 10 mg L^{-1} NAP solutions were added to the samples to determine the sorbent capacity in the real samples containing a high content of NAP. All the experiments were repeated three times under optimized conditions.

3. Results and discussion

3.1. Characterization

3.1.1. FTIR spectroscopy

The grafted functional groups and bonds on the Fe_3O_4 surface were identified and examined by FTIR spectroscopy. The FTIR adsorption is illustrated in Fig. 3.

3.1.1.1. Silica-coated magnetic nanoparticles

In the SCMNPs sample, the peak at 3,436 cm^{-1} is related to the O–H stretching vibrations of hydroxyl of adsorbed water [31]. The peak at 1,685 cm^{-1} can be ascribed to the out-of-plane bending of the O–H group of the adsorbed

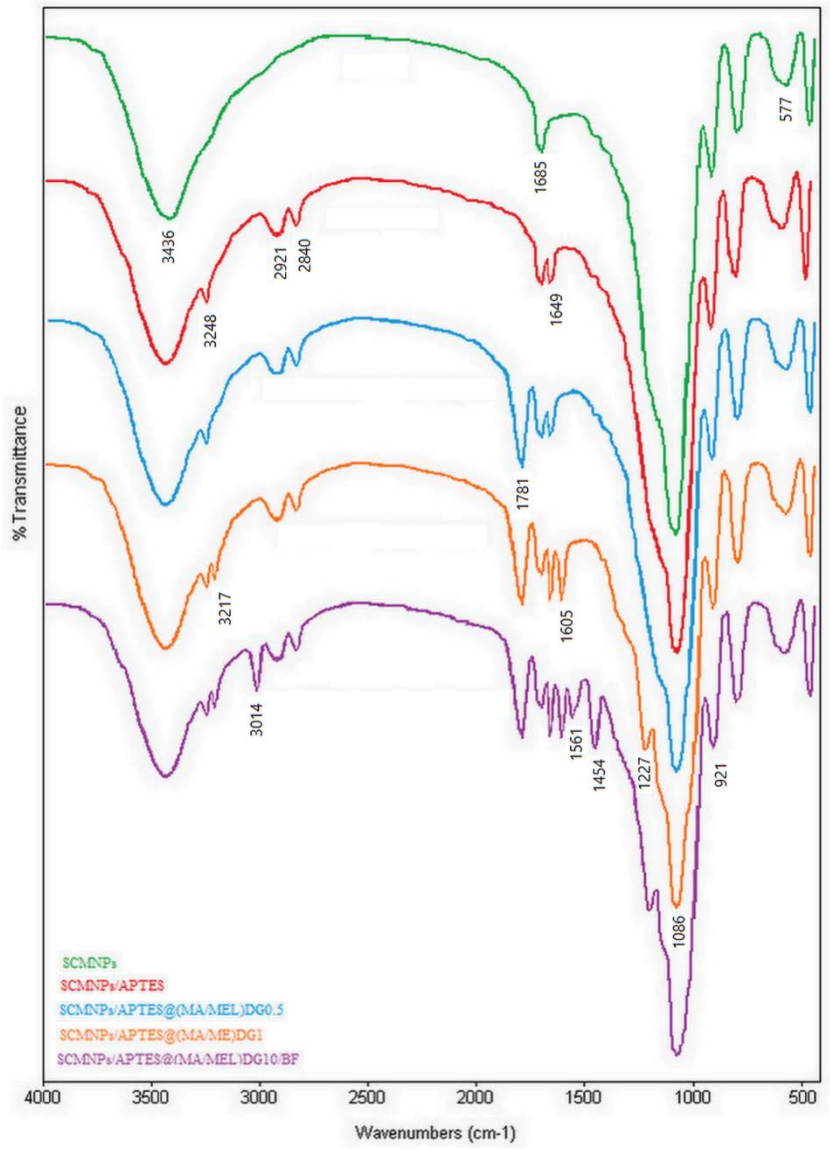

Fig. 3. FTIR spectra of SCMNPs, SCMNPs/APTES, SCMNPs/APTES@(MA)DG-0.5, SCMNPs/APTES@(MA/MEL)DG-1 and SCMNPs/APTES@(MA/MEL)DG-10/BF.

water [23,32]. The sharp peak at 1,086 cm^{-1} is related to the Si–O stretching, which shows the successful formation of SiO_2 layer on the MNPs [23]. The stretching adsorption of Si–OH appeared at 921 cm^{-1} [32]. The stretching vibrations at 577 cm^{-1} are ascribed to the Fe–O bonds confirming magnetic Fe_3O_4 particles [33].

3.1.1.2. SCMNPs/APTES

The vibrations at 1,649 and 3,248 cm^{-1} can be ascribed to the out-of-plane bending N–H and NH_2 groups in APTES [34]. The stretching vibrations at 2,840 and 2,921 cm^{-1} are assigned to the aliphatic bending mode of CH_2 groups on aminopropyl confirming APTES layer formation on the SCMNPs surface [35,36].

3.1.1.3. SCMNPs/APTES@(MA)DG-0.5

The stretching vibrations centered at 1,086 cm^{-1} confirm the Si–O bonding alongside the C–O formation in this step [23]. The band appearing at 1,781 cm^{-1} is ascribed to C=O, confirming the formation of half-generation dendrimer [32].

3.1.1.4. SCMNPs/APTES@(MA/MEL)DG-1

The peak obtained at 3,217 cm^{-1} and increasing intensity of peak 1,649 cm^{-1} can be attributed to the stretching and bending vibration of primary amine group H–N–H in MEL, respectively. The peaks obtained at 1,227 and 1,605 cm^{-1} are assigned to the stretching vibration of C–N and C=N respectively in triazine ring confirming MEL presence in the structure [37,38].

3.1.1.5. SCMNPs/APTES@(MA/MEL)DG-10/BF

The peak appearing at 1,454 cm^{-1} is attributed to the C=C in BF aromatic ring [39]. The aromatic skeletal vibrations are assigned to the peak at 1,561 cm^{-1}. The adsorption band 3,014 cm^{-1} is related to the aromatic C–H bonds in BF ligand [40].

3.1.2. Field-emission scanning electron microscopy

Field-emission scanning electron microscopy (FE-SEM) images were used to evaluate the nanostructure morphology and to measure the particle diameters (Fig. 4). Based on this figure, the average diameter of synthesized nanostructures was measured within the range of 20–70 nm. These particles have high porosity with spherical morphology. The particles are agglomerated but have a homogenous surface with reasonable dispersity in the matrix. High porosity in the sorbent structure enhances the interaction at the surface with the target NAP molecules for entrapment. Elemental analysis of the synthesized nanosorbent was obtained from EDS analysis in a random area of the sorbent surfaces.

The weight percentage of the elements present in the SCMNPs, SCMNPs/APTES, SCMNPs/APTES@(MA/MEL)DG-10, and SCMNPs/APTES@(MA/MEL)DG-10/BF nanoparticles are shown in Table 1. The presence of C, N, Fe, Si, and O obtained from EDS analysis confirms the successful formation of nanopolymer products. There is no value obtained for C and N elements in the SCMNPs sample. Increasing weight percentages of C and N values during polymerization from SCMNPs synthesis to SCMNPs/APTES@(MA/MEL)DG-10/BF step reveal effective bonding of APTES (silane groups), polymeric dendrimer chains and BF onto the MNPs surfaces. Reducing the Si and Fe weight percentages from SCMNPs synthesis step to SCMNPs/APTES@(MA/MEL)DG-10/BF as these two elements contained in the inner sites of adsorption, so their value decrease as the reactions proceed which also show successful progress in the synthetic routes.

3.1.3. XRD analysis

The XRD pattern of the nanostructured product is shown in Fig. 5. Comparing the obtained diffraction pattern for the sorbent product with the database (JCPDS 98-01101284) shows cubic crystals of MNPs with inverse spinal Fe_3O_4 structure. Also, comparing the position of peaks and the relative intensity of the obtained results with the reference pattern shows high purity Fe_3O_4 crystalline product. Common peaks for Fe_3O_4 position at 2θ, 30.32° (220), 35.651° (311), 43.27° (400), 53.81° (422), 57.26° (511) and 62.89° (440 confirmed the successful formation of magnetic core [41,42]. No additional peak observed for the product suggests the absence of any impurity in the sample during synthesis. In other words, the magnetite structure remained unaffected after coating with amorphous silica, silane groups, and dendrimer layers [32].

3.1.4. VSM spectrum

Changes in the SCMNPs magnetic properties (Fig. 6a) and SCMNPs/APTES@(MA/MEL)DG-10/BF nanopolymer (Fig. 6b) with the applied magnetic field at room temperature with the magnetic field of –15,000 to 15,000 Oe are shown in Fig. 6. This figure reveals the magnetization of the nanoparticles concerning the applied field magnitude. As shown in the figure, saturation magnetization (M_s) in Figs. 6a and b are 84 and 55 emu g^{-1} respectively. The obtained diagrams indicate that the magnetization diagram passes through the center, and there are no values obtained for the remnant-magnetization and coercivity. These confirm the super-magnetic properties of the nanoparticle products. The reduction in magnetic properties of Fig. 6b compared to Fig. 6a arises from reducing the magnetic momentum for the SCMNPs with non-magnetic APTES@(MA/MEL)DG-10/BF compound. AQ2

3.1.5. TGA analysis

Fig. 7 displays the thermal decomposition of nanostructured products of (a) SCMNPs (b) SCMNPs/APTES (c)

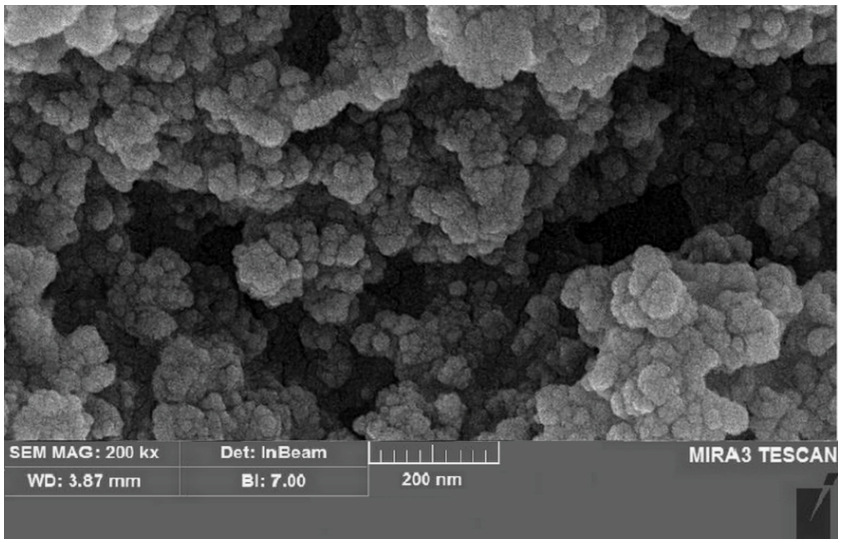

Fig. 4. SEM photograph of SCMNPs/APTES@(MA/MEL)DG-10/BF.

Table 1
EDS data of the elements in the nanostructure products

Samples	Weight (%) O	Weight (%) Si	Weight (%) Fe	Weight (%) N	Weight (%) C
SCMNPs	37	33	30	N.D.	N.D.
SCMNPs/APTES	28	26	23	2	21
SCMNPs/APTES@(MA/MEL)DG-10	20	13	13	29	25
SCMNPs/APTES@(MA/MEL)DG-10/BF	22	12	12	24	30

N.D.: Not detected.

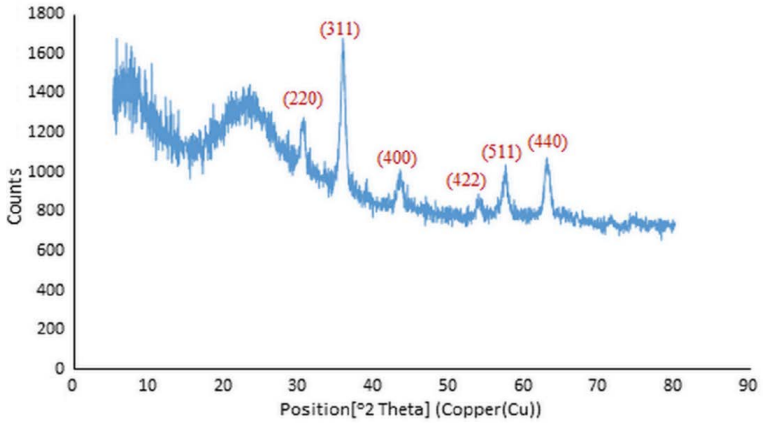

Fig. 5. XRD pattern of SCMNPs/APTES@(MA/MEL)DG-10/BF.

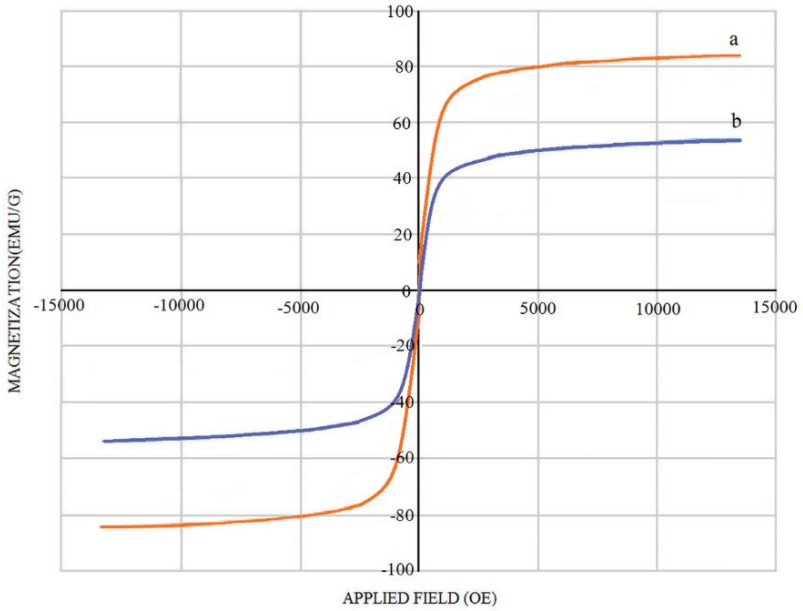

Fig. 6. VSM spectrum of (a) SCMNPs and (b) SCMNPs/APTES@(MA/MEL)DG-10/BF.

SCMNPs/APTES@(MA/MEL)DG-10/BF within the 0°C–600°C temperature in air atmosphere.

- SCMNPs graph shows a weight decline of 4.87% at 110°C. The weight reduction demonstrates the water-loss adsorbed on the surface. Due to the presence of the temperature stable inorganic compounds in the SCMNPs structure, negligible weight decline was observed in this graph.
- Alongside the weight loss for water molecules, the first weight loss occurred at 230°C, showing 8.57% weight reduction compared to the "*a*". This weight loss is related

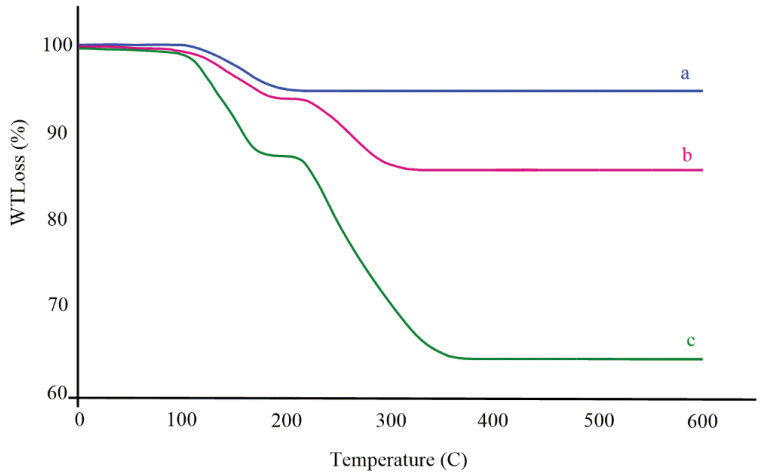

Fig. 7. Thermogravimetric analysis of (a) SCMNPs, (b) SCMNPs/APTES, and (c) SCMNPs/APTES@(MA/MEL)DG-10/BF.

to the thermal decomposition of APTES molecules and amine groups, also confirming the strong bonding of APTES on the SCMNPs surfaces.

- The first point that shows 6.42% weight loss compared to "*b*" observed at 110°C related to the water evaporation from the dendrimer layers and branches. The second weight loss occurred within the range of 230°C–320°C, which has 20.28% weight loss compared to the "*b*" indicating the thermal decomposition in the polymer matrices, dendrimer generations, and BF ligand. There is no significant weight loss above 400°C demonstrating enhanced thermal resistivity of the synthesized product.

The results from TGA analysis show that with increasing the number of dendrimer generations, the organic content grows accordingly. Successful modification of SCMNPs with APTES, dendrimer branches, and ligand was confirmed by the study of the thermograms obtained through TGA.

3.1.6. N_2 adsorption–desorption

N_2 adsorption–desorption analysis was used to evaluate the porous nature of synthesized nanoparticles. The BET analysis revealed that the surface area of SCMNPs/APTES@(MA/MEL)DG-10/BF was 115.17 $m^2\ g^{-1}$. The BJH calculation was performed to evaluate the pore volume and pore size distribution of the magnetic dendrimer. The results showed that the pore volume of the magnetic dendrimer was 0.44 $cm^3\ g^{-1}$ and its pore size was 10.15 nm.

3.2. Optimizing adsorption parameters

3.2.1. pH

The initial pH of the solution is a critical factor in the adsorption process in aqueous solution. The results from the pH effect on the NAP adsorption within the range of pH = 3–7 by SCMNPs/APTES@(MA/MEL)DG-10/BF sorbent product are shown in Fig. 8a. Other parameters including NAP concentration, temperature, contact time, and sorbent dosage remained constant as 20 mg L^{-1}, 25°C, 30 min, and 0.2 g L^{-1}, respectively. The obtained results showed that the highest adsorption occurred at pH = 7. So, neutral pH was chosen as an optimal operative parameter, which has also been reported for NAP in the literature [43,44]. The removal efficiency for NAP increased by changing the pH from 3 to 7 and indicated the highest removal at pH = 7 as 87.05%. Upon elevation of the pH value from neutral to alkaline (pH > 7), the removal efficiency decreased. This arises from the fact that NAP has different solubility at different pHs [45]. The pH of the solution can change the electrical charge of the sorbent surfaces, so at lower/higher pHs the removal efficiency decreases. Also, there are no functional groups on the surface of these poly-aromatic compounds. Neutral pH as an optimized parameter for the adsorption of NAP by the sorbent product has a benefit of rapid adsorption process as there is no need for sample preparation and pH adjustment for real samples in the contaminated water. In the subsequent studies, pH = 7 was used as optimized.

The pH_{PZC} of the adsorbent was obtained in the range of 7. Thus, the adsorbent surface charge is neutral at pH equal to 7, it is also positive at pH < 7 bar and negative at pH > 7. The point of zero charge (pH_{PZC}) confirms the mechanism of the adsorption. NAP is a non-ionized and nonpolar aromatic compound. Since the surface charge of the adsorbent and the NAP solution are both neutral at the pH value of 7, therefore, the highest absorption rate was achieved. The optimum adsorption of NAP occurred at pH 7 after which the adsorbent had no more affinity. Rapid adsorption of NAP can be attributed to intermolecular forces, hydrophobic bonding, and binding sites on the dendrimer. So, hydrophobic bonding and dispersive interactions are more effective driving forces as compared to electrostatic force for NAP adsorbtion onto the nanopolymer at neutral pH.

3.2.2. Sorbent dosage

To obtain the optimum sorbent dosage, NAP solutions (20 mg L^{-1}) at pH = 7 were prepared, and different dosages of the sorbent (0.01–2.0 g L^{-1}) were added to the above solutions and shaken for 30 min at 25°C (Fig. 8b).

With an increase in the sorbent dosage from 0.01 to 2.0 g L^{-1}, the available adsorption sites along the active

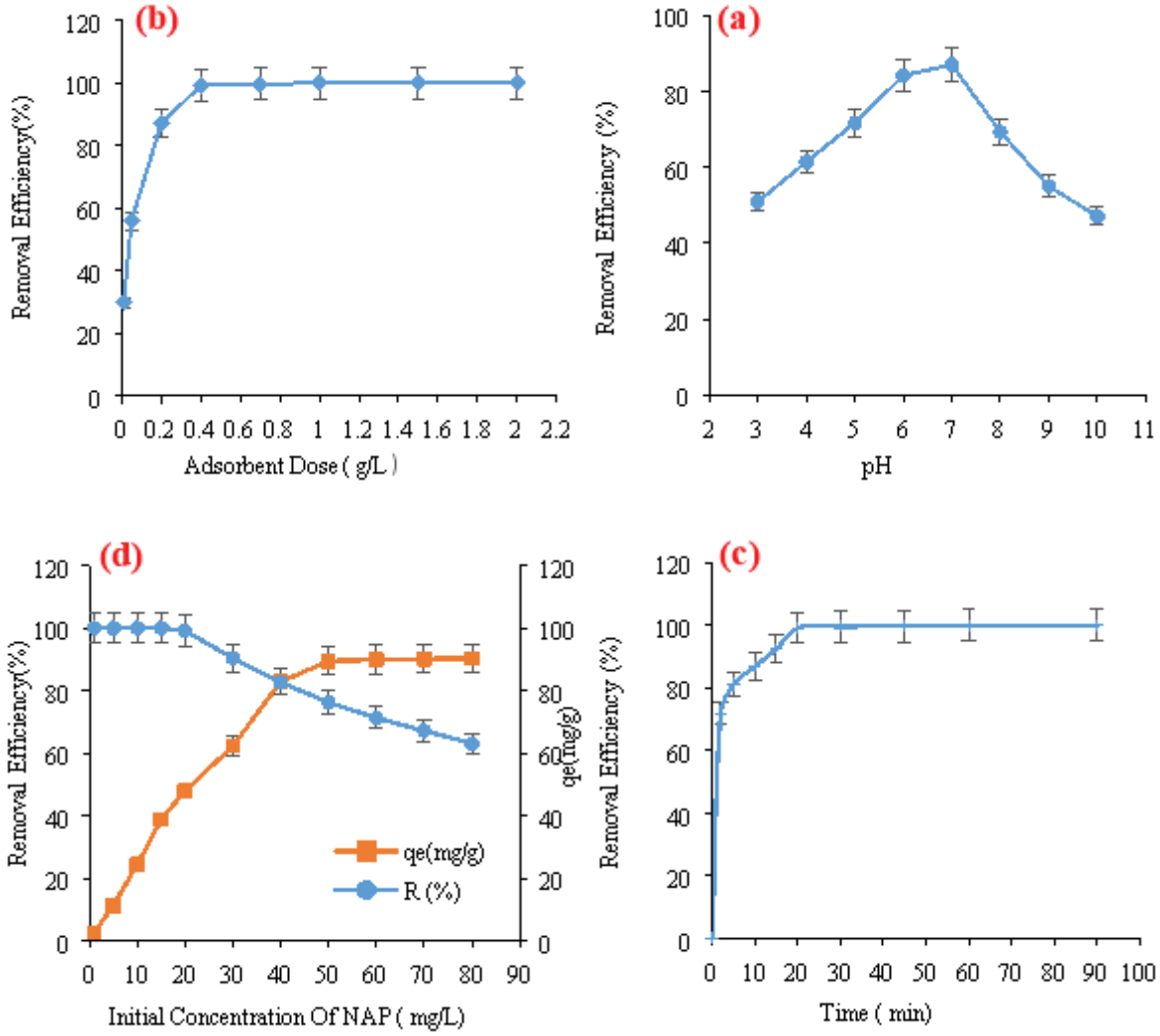

Fig. 8. Optimizing the adsorption parameters (a) pH, (b) sorbent dosage, (c) contact time, and (d) initial concentration of NAP.

surfaces increased, and the removal efficiency grew accordingly [43,46]. At the 0.4 g L^{-1} of the sorbent concentration, the diagram reached equilibrium, so there were no significant changes for the 0.4–2.0 g L^{-1} of the sorbent dosage. The optimum 0.4 g L^{-1} was used in the subsequent studies.

3.2.3. Contact time

In this series of experiments, the effect of contact time was investigated on adsorption (2–90 min) at an initial NAP concentration of 20 mg L^{-1}. The pH and adsorbent concentration were also considered at the optimal state at 25°C (Fig. 8c). Although the removal of the NAP increased with time, the rate of the adsorption diminished. The removal of NAP by the nanopolymer was very high in the early minutes of the adsorption process, such that 71.84% of NAP was removed by the nanopolymer within the first 2 min of reaction. There was rapid adsorption at the initial stage of the process, which diminished gradually and reached a constant value at equilibrium. The results showed that NAP removal reached its maximum at 20 min. The PAHs removal by the nanopolymer at the initial stage of the process occurred in the active sites at the surfaces. These active sites were occupied gradually until the sorbent became saturated [16,47].

3.2.4. NAP concentration

To evaluate this, different concentrations of NAP solutions (1–80 mg L^{-1}) were prepared, while the other parameters remained constant at their optimized values. The results obtained in Fig. 8d shows that the synthetic nanopolymer can remove the low concentration of NAP completely, but the removal efficiency decreases as the NAP concentration increases. At low concentrations, the number of NAP molecules is less compared to the available sites on the nanosorbent, so the removal efficiency is high. Upon elevation of the NAP concentration (as the number of active sites remains unchanged), NAP content shrinks compared to the empty sites, thus reducing the removal efficiency. Despite this fact, there is a different trend in the adsorption process as the sorption capacity increased by raising the NAP concentration [45]. The larger sorption capacity

at higher concentrations can be a consequence of the unsaturation of the surface at lower concentrations. The sorption capacity of the magnetic nanostructure grew from 2.475 mg g^{-1} at 1 mg L^{-1} NAP to 89.412 mg g^{-1} at 50 mg L^{-1} of NAP concentration. As illustrated in Fig. 8d, the sorption capacity of the magnetic nanostructure increased with the initial concentration of NAP and reached a plateau value (in 50 mg L^{-1} NAP concentration) [48].

3.2.5. Temperatures

The adsorption of NAP on the nanopolymer was investigated within the temperature range of 15°C–45°C under optimum conditions (pH = 7, 0.4 g L^{-1} sorbent dosage, 20 min, 20 mg L^{-1} NAP concentration). Removal efficiency for temperatures of 15°C, 20°C, 25°C, 30°C, 35°C, 40°C, and 45°C obtained as 84.60%, 92.58%, 100%, 93.12%, 85.76%, 77.35%, and 70.09% respectively. With the increase of the temperature from 15°C to 25°C, the removal efficiency increased. In this study, the temperature ranges of 25°C was considered as the optimum temperature and indicated that the optimum reaction can be carried out at room temperature. At higher temperatures of about 35°C–45°C, the adsorption forces between the aromatic hydrocarbon molecules and the active sites of the adsorbent surface became weaker and the removal percentage diminished.

3.3. Desorption and repeated use

In this study, the adsorption-desorption cycle was repeated 10 times (under optimum conditions). The removal efficiency for the first cycle to the fifth cycle was obtained as 100%, 99.16%, 97.43%, 94.78%, and 91.23% respectively. Note that up to the initial five cycles, the removal efficiency showed more than 90% removal. In subsequent cycles (fifth cycle to the tenth cycle) the percentage of NAP removal decreases. The NAP removal efficiency decreased from about 91.23% in the fifth cycle to about 59.3% in the tenth cycle. The reduction in the removal efficiency can be ascribed to the lessening of the active sites on the sorbent surfaces.

3.4. Comparison of the removal efficiency for NAP in different sorbents with this work

The NAP removal efficiency has been compared for different synthetic nanostructures in a series of experiments. The results are presented in Table 2. The results show that by forming the polymeric dendrimer on the magnetic core surface, the removal efficiency for NAP rises. Also, by increasing the number of dendrimer generations and ligand containing a benzene ring, the highest value is obtained for NAP removal.

Table 2
Relative sorption value of NAP by prepared sorbents in this work

Sorbent	Relative sorption value of NAP (%)
SCMNPs	20.88
SCMNPs/APTES	21.70
SCMNPs/APTES@(MA/MEL)DG-5	57.14
SCMNPs/APTES@(MA/MEL)DG-10	90.57
SCMNPs/APTES@(MA/MEL)DG-10/BF	100

3.5. Method application

To provide evidence on the capability of the synthesized magnetic dendrimer, and evaluate the strategy, as well as reliability of the suggested method, real samples (river water, seawater, and industrial waste), were provided and studied. The NAP content in these samples was measured by the GC-MS technique. This technique can measure trace organic compounds remaining in solutions. Seawater was provided from Guilan-Tehran River, seawater from Caspian Sea-Iran, and industrial waste from the coal industry. To measure the samples accurately, each test was repeated three times with GC-MS, with the results shown in Table 3. The presence of other elements and compounds in real water, especially from the industrial waste which contains complex matrices, reduces the NAP removal efficiency. These compounds act as a competitive species to occupy the active sites on the sorbent. Nevertheless, the NAP removal efficiency by the synthetic nanocomposite was high enough and suggested the capability of the suggested method for real samples.

3.6. Isotherm models

Adsorption isotherms can describe the adsorption mechanism of the adsorbate with sorbent based on the equilibrium data and adsorption properties and can determine the sorbent capacity. In this work, the equilibrium adsorption of NAP with synthesized SCMNPs/APTES@(MA/MEL)DG-10/BF sorbent was studied by Langmuir, Freundlich, Temkin, and Redlich–Peterson isotherms. Langmuir isotherm assumes monolayer adsorption of the targeted adsorbate on the outer surface of the adsorbent [49]. The equation of the Langmuir isotherm is proposed as a linear form as below [50–52]:

$$\frac{C_e}{q_e} = \frac{C_e}{q_{\max}} + \frac{1}{q_{\max} K_L} \tag{3}$$

where K_L (L mg^{-1}) denotes the equilibrium constant, q_m (mg g^{-1}) is the maximum adsorption capacity in the monolayer adsorption process, C_e (mg L^{-1}) represents the NAP concentration at the equilibrium, and q_e (mg g^{-1}) is the NAP content per mass of the sorbent. The $1/q_m$ value represents the slope of the line, and $1/K_L\ q_m$ is the intercept. Using the R_L parameter (separation factor), one can determine the type of the process. A favorable value for R_L is 0–10 (Eq. (4)) [51,53,54]:

$$R_L = \frac{1}{1 + K_L \times C_0} \tag{4}$$

Multi-layer adsorption isotherm for the heterogeneous surfaces is represented by Freundlich [55]. The linear equation of this model can be seen in Eq. (5) [56]:

Table 3
NAP sorption values by the sorbent product in the real samples

No.	Samples	Found (mg L^{-1})	Added (mg L^{-1})	Residual (mg L^{-1})	Removal (%)	Relative standard deviation (%)
1	River water	0.00092	–	N.D.	100	–
2	River water	0.00092	2	N.D.	100	–
3	Seawater	0.0074	–	N.D.	100	–
4	Seawater	0.0074	5	N.D.	100	–
5	Industrial wastewater	20.455	–	1.967	90.38	0.08
6	Industrial wastewater	20.455	10	4.348	85.72	0.06

N.D.: Not detected.

AQ3

$$\ln q_e = \ln K_F + \frac{1}{n}\ln C_e \quad (5)$$

where n is the Freundlich constant representing the regression slope of the linear form of the model and K_F (mg g^{-1}) (L $mg^{-1})^{1/n}$ is the intercept of the Freundlich model.

In the Temkin model [Eq. (6)], heat adsorption drops linearly, demonstrating the sorbent–adsorbate interactions. It occurs when the number of adsorbed particles increases on the sorbent surfaces [57,58]:

$$q_e = B \ln C_e + B \ln A \quad (6)$$

where A (L mg^{-1}) is the bonding/fixed constant and $B = RT/b$. T denotes the absolute temperature (K), R (8.314 J mol^{-1} K) is the global gas constant, and b (J mol^{-1}) is the adsorption heat.

Redlich–Peterson is the combinational model of the Langmuir and Freundlich models as a compromising model between homogeneous and heterogeneous adsorption. This model can determine the adsorption interaction parameters in a wide range of concentrations [55,59]. By obtaining $\ln[A(C_e/q_e)-1]$ values and plotting vs. $\ln C_e$ the parameters can be found. The linear equation of the Redlich–Peterson model is shown in Eq. (7) [60]:

$$\ln\left(A \cdot \frac{C_e}{q_e} - 1\right) = g \ln C_e + \ln B \quad (7)$$

where A (L g^{-1}) and B (J mol^{-1}) are the constants of the model and g denotes A dimensionless parameter which is in the range of $0 < g \leq 1$. The tendency of g value toward zero shows the data follow the Freundlich model, as the tendency toward one is suggestive of the Langmuir model [55,60].

The parameters calculated from the isotherm models and their regression are presented in Table 4 and Fig. 9. Studies of the adsorption models show that the dominant model for NAP sorption in this system follows the Langmuir model (R^2 = 0.9969). Also, considering g = 1 value from the Freundlich–Peterson model, it can be stated that data are compatible with the Langmuir model and the majority of the adsorption process occurs in mono-layer formation. π–π interactions between NAP molecules and sorbent product surfaces cause dispersion and enhance the NAP adsorption capacity onto the sorbent. Also, the results obtained from Langmuir show that the R_L coefficient lied within the favorable range (0–1) as R_L = 0.0168. Thus, the value of R_L is favorable and the absorption process is successful. The q_m is calculated as q_m = 94.33 mg g^{-1} stating that 1 g of individual sorbent could adsorb 94.33 mg of the NAP, which is an excellent result.

3.7. Comparison of the maximum NAP adsorption of Ps/APTES@(MA/MEL)DG-10/BF by other sorbents

Table 5 summarizes the maximum NAP adsorption capacity of the sorbent product synthesized in this study, as well as others reported in the literature.

As seen, the nanopolymer fabricated in this study has the highest adsorption capacity among the other reported sorbents for NAP removal owing to the surface modification and advance polymerization technique.

3.8. Adsorption kinetic studies

The kinetics of the reaction should be evaluated to provide information about operating parameters affecting the adsorption and demanding time for the reaction reaching the equilibrium [55]. In this study, pseudo-first-order, pseudo-second-order, and intraparticle models were studied. Eq. (8) shows the linear form of the pseudo-first-order model [64,65]:

$$\log\left(q_e - q_t\right) = \log q_e - \frac{k_1}{2.303} t \quad (8)$$

where q_e and q_t (mg g^{-1}) denote the NAP adsorbed in the equilibrium and time t, t is the adsorption time (min), k_1 (min^{-1}) shows the model constant. k_1 and q_t are the slope and the intercept of the regression line, respectively.

The following equation shows the pseudo-second-order model [Eq. (9)] [43,66]:

$$\frac{t}{q_t} = \frac{1}{k_2 q_e^2} + \frac{t}{q_e} \quad (9)$$

where k_2 (g $mg^{-1}min^{-1}$) denotes the model constant. In this model, by calculating t/q_t vs. t, k_2 and q_e can be calculated.

Intraparticle diffusion kinetic model (Weber–Morris) studies the mechanism of the adsorbate in the porous sorbent as follows [64–66]:

Table 4
Calculated parameters from isotherm models in this study

Isotherm model	Parameter	Quantity	Isotherm model	Parameter	Quantity
Langmuir	q_{max} (mg g^{-1})	94.34	Temkin	A (L g^{-1})	16.36
	K_L (L mg^{-1})	1.16		B	17.1
	R_L	0.017		b (J mol^{-1})	144.9
	R^2	0.9969		R^2	0.9867
Freundlich	K_F (mg g^{-1})(L mg^{-1})$^{1/n}$	43.5	Redlich–Peterson	A	112
	n	3.04		B	1.2
	R^2	3.04		g	1.009
				R^2	0.9966

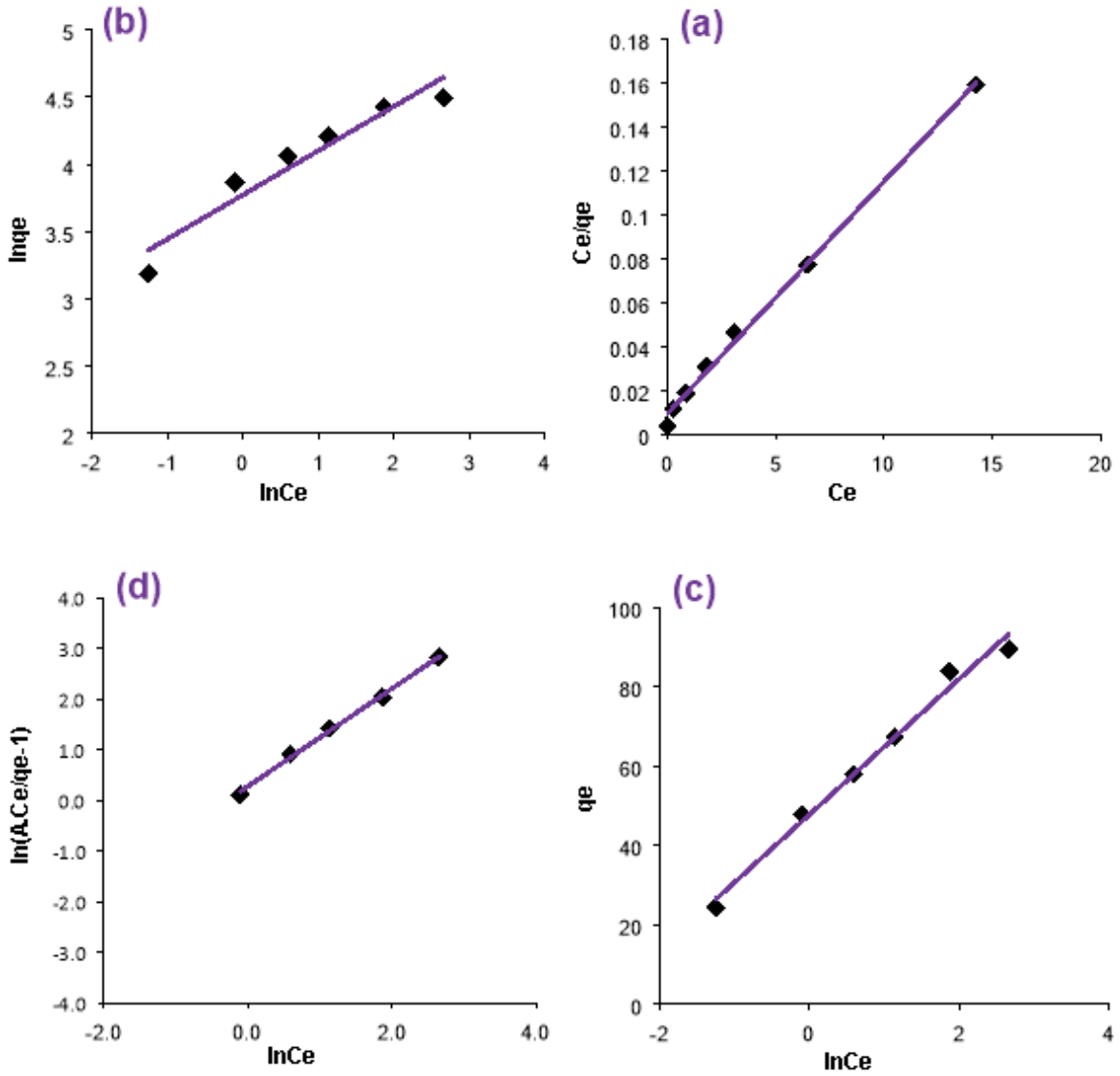

Fig. 9. Regression of isotherm models: (a) Langmuir, (b) Freundlich, (c) Temkin, and (d) Redlich–Peterson (pH = 7; 20 min; 150 rpm; 1–50 mg L^{-1} NAP; 0.4 g L^{-1} sorbent, at 25°C).

Table 5
Comparison of the maximum adsorption capacity (q_m) for naphthalene with other reported sorbents in the literature

No.	Adsorbent	q_m (mg g^{-1})	pH	Sorbent dosage (g L^{-1})	NAP concentration (mg L^{-1})	T (°C)	References
1	SCMNPs/APTES@ (MA/MEL) DG-10/BF	94.339	7	0.4	20	25	This study
2	HB[a]	22.45	5.97	1	10	20	[7]
3	Graphene oxide	3.3308	7	2	–	30	[43]
4	Graphene	5.9880	6	2	–	30	[43]
5	MB500[b]	21.692	7.5	4	50	28	[51]
6	PMO[c]	46.641	–	5	10	28	[55]
7	TX100[d] impregnated into chitosan beads	32.39	6	0.6	15	30	[61]
8	CTAB[e] impregnated into chitosan beads	31.77	6	0.5	15	30	[61]
9	SDS[f] impregnated into chitosan beads	28.66	6	0.8	15	30	[61]
10	xGnP[g]	0.00162	7	0.4	–	25	[62]
11	Kaolinite modified by HDTMA[h]	21.02	6.8	–	25	25	[63]
12	Halloysite modified by HDTMA[i]	28.45	6.8	–	25	25	[63]

[a]Hexadecyltrimethylammonium bromide modified bentonite
[b]Activated carbon produced from milk bush kernel shell
[c]Periodic mesoporous organosilica
[d]Triton X-100 (a type of surfactant)
[e]Cetyl trimethyl ammonium bromide (a type of surfactant)
[f]sodium dodecyl sulfate (a type of surfactant)
[g]Exfoliated graphite nanoplatelets
[h]Hexadecyltrimethylammonium
[i]Hexadecyltrimethylammonium

$$q_t = k_p t^{0.5} + C \tag{10}$$

where k_p (mg g^{-1} min$^{-1(1/2)}$) represents the dispersion rate constant in the particle, C is the constant for mass transfer in each experiment because of the boundary layer thickness.

Chrastil's diffusion model describes sorption kinetics in controlled diffusion systems [67]:

$$q_t = q_e\left(1 - e^{-k_c A_0 t}\right)^n \tag{11}$$

where k_c (L g^{-1} min^{-1}) is a rate constant, which depends on diffusion coefficients and sorption capacity of sorbent. A_0 (g L^{-1}) refers to the dose of the sorbent. n is a heterogeneous structural diffusion resistance constant ($0 < n < 1$). The constant n is independent of the NAP concentration, sorbent concentration A_0, q_e, or temperature.

The parameters calculated from these four kinetic models are presented in Table 6 as well as the pseudo-second-order and intraparticle diffusion kinetic regression lines in Fig. 10. The results from the kinetic studies show that the data follow the order of pseudo-first-order < Chrastil's diffusion < intraparticle diffusion < pseudo-second-order. A comparison of the R-squared value of the diagrams reveals that the pseudo-second-order model (R^2 = 0.999) designates better fitness of experimental data with the model. As a result, chemical bonding formation in this process is the dominant mechanism for the sorption process and occurs chemically.

Table.6
Kinetic parameters for NAP adsorption onto the prepared sorbent

Kinetic model	Parameter	Quantity
Pseudo-first-order	q_e (mg g^{-1})	12.508
	k_1 (min^{-1})	0.0868
	R^2	0.9436
Pseudo-second-order	q_e (mg g^{-1})	48.780
	k_2 (g mg^{-1} min^{-1})	0.019
	R^2	0.9998
Intraparticle diffusion	k_p (mg g^{-1} min$^{-1\,(1/2)}$)	4.108
	c	29.142
	R^2	0.9903
Chrastil's diffusion	q_e (mg g^{-1})	48.514
	k_c (L g^{-1} min^{-1})	0.1743
	n	0.1721
	R^2	0.9752

4. Conclusions

In this study, the successful synthesis of the novel MNPs was reported through continuous polymerization and formation of a higher generation of dendrimers further enhanced by the covalent bonding of the ligands on the surface. It showed high adsorption capability for non-saturated

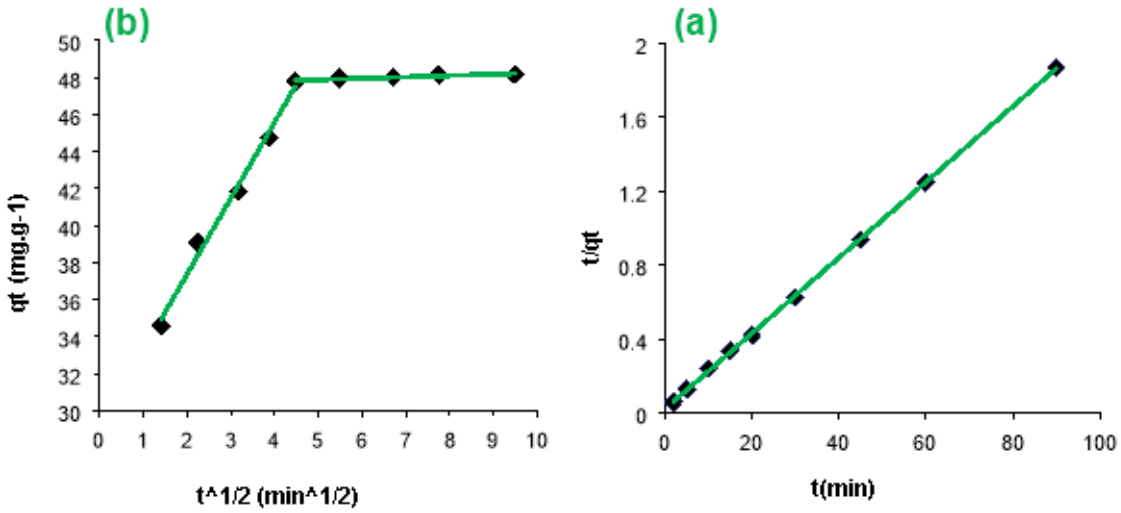

Fig. 10. Kinetic regression lines (a) pseudo-second-ordera and (b) intraparticle diffusion (pH = 7; 2–90 min–150 rpm; 20 mg L^{-1} NAP; 0.4 g L^{-1} sorbent, at 25°C).

organic compounds (i.e., NAP). The high adsorption capacity was owing to the magnetite core with super-magnetic properties and enhanced inner active sites due to the ten-generation dendrimer and high-ordered network structure of the highly branched polymer. Additionally, terminal ligand containing benzene ring enhanced the π–π interactions between NAP molecules and the sorbent surfaces, boosting the adsorption capacity. Data analysis and high removal efficiency in industrial wastewater and natural water samples indicated that using of GC-MS technique is appropriate in this process. The sorbent product was characterized by FTIR, FE-SEM-EDS, TGA, XRD, and VSM with the results confirming the successful fabrication of the sorbent product. The maximum adsorption (>99%) at optimal conditions was obtained for 0.4 g L^{-1} of sorbent and 15 mg L^{-1} of NAP concentration at pH = 7. The adsorption reaction reached equilibrium at 20 min. Studies from different isotherm models showed that the process follows the Langmuir model (R^2 = 0.9969) with the pseudo-second-order kinetics (R^2 = 0.9998). The adsorption capacity of the prepared nanocomposite was 94.33 mg g^{-1} which had a higher potential for the application compared to the reported sorbents in the literature [7,43,51,55,61–63]. Other substantial properties of the sorbent such as recovery rate, reusability during several sorption processes alongside the low-cost, chemically stable, high rate reaction, high adsorption capacity and simple separation method by external magnetic field confirm that SCMNPs/APTES@(MA/MEL)DG-10/BF sorbent has the capability for removing aromatic hydrocarbons (i.e., NAP) from aqueous samples.

References

[1] S.M. Yakout, A.A.M. Daifullah, S.A. El-Reefy, Adsorption of naphthalene, phenanthrene and pyrene from aqueous solution using low-cost activated carbon derived from agricultural wastes, Adsorpt. Sci. Technol., 31 (2013) 293–302.
[2] E.R.L. Tiburtius, P. Peralta-Zamora, A. Emmel, Treatment of gasoline-contaminated waters by advanced oxidation processes, J. Hazard. Mater., 126 (2005) 86–90.
[3] Y. Huang, A.N. Fulton, A.A. Keller, Simultaneous removal of PAHs and metal contaminants from water using magnetic nanoparticle adsorbents, Sci. Total Environ., 571 (2016) 1029–1036.
[4] H. Gupta, Anthracene removal from water onto activated carbon derived from vehicular tyre, Sep. Sci. Technol., 53 (2018) 613–625.
[5] B. Gupta, H. Gupta, Iron oxide mediated degradation of mutagen pyrene and determination of degradation products, Int. J. Environ. Sci. Dev., 6 (2015) 908–912.
[6] X. Yang, J. Li, T. Wen, X. Ren, Y. Huang, X. Wang, Adsorption of naphthalene and its derivatives on magnetic graphene composites and the mechanism investigation, Colloids Surf., A, 422 (2013) 118–125.
[7] E.M.Ö. Kaya, A.S. Özcan, Ö. Gök, A. Özcan, Adsorption kinetics and isotherm parameters of naphthalene onto natural- and chemically modified bentonite from aqueous solutions, Adsorption, 19 (2013) 879–888.
[8] R.S. DeFever, N.K. Geitner, P. Bhattacharya, F. Ding, P.C. Ke, S. Sarupria, PAMAM dendrimers and graphene: materials for removing aromatic contaminants from water, Environ. Sci. Technol., 49 (2015) 4490–4497.
[9] A.A. Daifullah, B. Girgis, Impact of surface characteristics of activated carbon on adsorption of BTEX, Colloids Surf., A, 214 (2003) 181–193.
[10] M. Faraji, Y. Yamini, A. Saleh, M. Rezaee, M. Ghambarian, R. Hassani, A nanoparticle-based solid-phase extraction procedure followed by flow injection inductively coupled plasma-optical emission spectrometry to determine some heavy metal ions in water samples, Anal. Chim. Acta, 659 (2010) 172–177.
[11] C. Huang, B. Hu, Silica-coated magnetic nanoparticles modified with γ-mercaptopropyltrimethoxysilane for fast and selective solid phase extraction of trace amounts of Cd, Cu, Hg, and Pb in environmental and biological samples prior to their determination by inductively co, Spectrochim. Acta, Part B, 63 (2008) 437–444.
[12] S. Shariati, M. Faraji, Y. Yamini, A.A. Rajabi, Fe_3O_4 magnetic nanoparticles modified with sodium dodecyl sulfate for removal of safranin O dye from aqueous solutions, Desalination, 270 (2011) 160–165.
[13] J.H. Jang, H.B. Lim, Characterization and analytical application of surface modified magnetic nanoparticles, Microchem. J., 94 (2010) 148–158.
[14] A.A. Al-rashdi, Double-functionalized magnetic nanoparticles for preconcentration and determination of polycyclic aromatic hydrocarbons in water samples, Anal. Chem. Res., 10 (2016) 9–17.

[15] E. Abbasi, S. Aval, A. Akbarzadeh, M. Milani, H. Nasrabadi, S. Joo, Y. Hanifehpour, K. Nejati-Koshki, R. Pashaei-Asl, Dendrimers: synthesis, applications, and properties, Nanoscale Res. Lett., 9 (2014) 247.
[16] M. Sajid, M.K. Nazal, Ihsanullah, N. Baig, A.M. Osman, Removal of heavy metals and organic pollutants from water using dendritic polymers based adsorbents: a critical review, Sep. Purif. Technol., 191 (2018) 400–423.
[17] S. Charles, N. Vasanthan, D. Kwon, G. Sekosan, S. Ghosh, Surface modification of poly(amidoamine) (PAMAM) dendrimer as antimicrobial agents, Tetrahedron Lett., 53 (2012) 6670–6675.
[18] Y. Liu, V.S. Bryantsev, M.S. Diallo, W.A. Goddard III, PAMAM dendrimers undergo pH responsive conformational changes without swelling, J. Am. Chem. Soc., 131 (2009) 2798–2799.
[19] E. Vunain, A. Mishra, B. Mamba, Dendrimers, mesoporous silicas and chitosan-based nanosorbents for the removal of heavy-metal ions: a review, Int. J. Biol. Macromol., 86 (2016) 570–586.
[20] C.M. Chou, H.L. Lien, Dendrimer-conjugated magnetic nanoparticles for removal of zinc(II) from aqueous solutions, J. Nanopart. Res., 13 (2011) 2099–2107.
[21] M. Sajid, C. Basheer, Layered double hydroxides: emerging sorbent materials for analytical extractions, TrAC, Trends Anal. Chem., 75 (2016) 174–182.
[22] R.M. Triano, M.L. Paccagnini, A.M. Balija, Effect of dendrimeric composition on the removal of pyrene from water, Springerplus, 4 (2015) 511.
[23] S. Aliannejadi, A.H. Hassani, H.A. Panahi, S.M. Borghei, Fabrication and characterization of high-branched recyclable PAMAM dendrimer polymers on the modified magnetic nanoparticles for removing naphthalene from aqueous solutions, Microchem. J., 145 (2019) 767–777.
[24] S. Chandra, G. Noronha, S. Dietrich, H. Lang, D. Bahadur, Dendrimer-magnetic nanoparticles as multiple stimuli responsive and enzymatic drug delivery vehicle, J. Magn. Magn. Mater., 380 (2015) 7–12.
[25] M. Gao, W. Li, J. Dong, Z. Zhang, B. Yang, Synthesis and characterization of superparamagnetic Fe_3O_4@SiO_2 core-shell composite nanoparticles, World J. Condens. Matter Phys., 1 (2011) 49–54.
[26] M. Jafarzadeh, E. Soleimani, P. Norouzi, R. Adnan, H. Sepahvand, Preparation of trifluoroacetic acid-immobilized Fe_3O_4@SiO_2–APTES nanocatalyst for synthesis of quinolines, J. Fluorine Chem., 178 (2015) 219–224.
[27] R.B. Yang, P.M. Reddy, C.J. Chang, P.A. Chen, J.K. Chen, C.C. Chang, Synthesis and characterization of Fe_3O_4/polypyrrole/carbon nanotube composites with tunable microwave absorption properties: role of carbon nanotube and polypyrrole content, Chem. Eng. J., 285 (2016) 497–507.
[28] L. Subbiah, S. Palanisamy, B.T. Sivaprakasam, D. Elamurugan, Synthesis and evaluation of polyamidoamine (Pamam) dendrimer as a carrier of cefixime drug, World J. Pharm. Pharm. Sci., 5 (2016) 858–867.
[29] M. Kostić, J. Mitrović, M. Radović, M. Đorđević, Mi. Petović, D. Bojić, A. Bojić, Effects of power of ultrasound on removal of Cu(II) ions by xanthated *Lagenaria vulgaris* shell, Ecol. Eng., 90 (2016) 82–86.
[30] A.E. Yayayürük, O. Yayayürük, Facile synthesis of magnetic iron oxide coated amberlite XAD-7HP particles for the removal of Cr(III) from aqueous solutions: sorption, equilibrium, kinetics and thermodynamic studies, J. Environ. Chem. Eng., 7 (2019) 103145.
[31] H. Yang, H. Li, J. Zhai, L. Sun, Y. Zhao, H. Yu, Magnetic prussian blue/graphene oxide nanocomposites caged in calcium alginate microbeads for elimination of cesium ions from water and soil, Chem. Eng. J., 246 (2014) 10–19.
[32] Y. Wang, P. Su, S. Wang, J. Wu, J. Huang, Y. Yang, Dendrimer modified magnetic nanoparticles for immobilized BSA: a novel chiral magnetic nano-selector for direct separation of racemates, J. Mater. Chem. B, 1 (2013) 5028–5035.
[33] B.-F. Pan, F. Gao, H.-C. Gu, Dendrimer modified magnetite nanoparticles for protein immobilization, J. Colloid Interface Sci., 284 (2005) 1–6.
[34] K.S. Aneja, S. Bohm, A.S. Khanna, H.L.M. Bohm, Graphene based anticorrosive coatings for Cr(VI) replacement, Nanoscale, 7 (2015) 17879–17888.
[35] S. Chen, J. Hong, H. Yang, J. Yang, Adsorption of uranium(VI) from aqueous solution using a novel graphene oxide-activated carbon felt composite, J. Environ. Radioact., 126 (2013) 253–258.
[36] P. Sharma, B.K. Saikia, M.R. Das, Removal of methyl green dye molecule from aqueous system using reduced graphene oxide as an efficient adsorbent: kinetics, isotherm and thermodynamic parameters, Colloids Surf., A, 457 (2014) 125–133.
[37] F. Ma, H. Zhao, L. Sun, Q. Li, L. Huo, T. Xia, S. Gao, G. Pang, Z. Shi, S. Feng, A facile route for nitrogen-doped hollow graphitic carbon spheres with superior performance in supercapacitors, J. Mater. Chem., 22 (2012) 13464.
[38] F. Jiryaei Sharahi, A. Shahbazi, Melamine-based dendrimer amine-modified magnetic nanoparticles as an efficient Pb(II) adsorbent for wastewater treatment: adsorption optimization by response surface methodology, Chemosphere, 189 (2017) 291–300.
[39] J. Blažević, L. Colombo, The vibrational spectrum of the benzophenone molecule, J. Raman Spectrosc., 11 (1981) 143–149.
[40] N.K. Ladani, M.P. Patel, R.G. Patel, A convenient one-pot synthesis of series of 3-(2,6-diphenyl-4-pyridyl)hydroquinolin-2-one under microwave irradiation and their antimicrobial activities, Indian J. Chem., 48B (2009) 261266.
[41] A. Demir, A. Baykal, H. Sözeri, R. Topkaya, Low temperature magnetic investigation of Fe_3O_4 nanoparticles filled into multiwalled carbon nanotubes, Synth. Met., 187 (2014) 75–80.
[42] A. Maleki, R. Rahimi, S. Maleki, Preparation and characterization of magnetic chlorochromate hybrid nanomaterials with triphenylphosphine surface-modified iron oxide nanoparticles, J. Nanostruct. Chem., 4 (2014) 153–160.
[43] P. Das, S. Goswami, S. Maiti, Removal of naphthalene present in synthetic waste water using novel graphene/graphene oxide nano sheet synthesized from rice straw: comparative analysis, isotherm and kinetics, Front. Nanosci. Nanotechnol., 2 (2016) 38–42.
[44] N. Budhwani, Removal of polycyclic aromatic hydrocarbons present in tyre pyrolytic oil using low cost natural adsorbents, Environ. Ecol. Eng., 9 (2015) 186–190.
[45] S.S.M. Hassan, H.I. Abdel-Shafy, M.S.M. Mansour, Removal of pyrene and benzo(a)pyrene micropollutant from water via adsorption by green synthesized iron oxide nanoparticles, Adv. Nat. Sci. Nanosci. Nanotechnol., 9 (2018) 015006.
[46] H. Gupta, R. Kumar, Removal of PAH anthracene from aqueous media using banana peel activated carbon, Int. J. Sci. Res. Environ. Sci., 4 (2016) 109–114.
[47] A. Pourjavadi, A. Abedin-Moghanaki, S.H. Hosseini, Synthesis of poly(amidoamine)-graft-poly(methyl acrylate) magnetic nanocomposite for removal of lead contaminant from aqueous media, Int. J. Environ. Sci. Technol., 13 (2016) 2437–2448.
[48] O. Yayayuruk, Sorption of cationic and anionic dyes using poly (acrylamide) grafted onto cross-linked poly (4-vinyl pyridine) from aqueous solutions, J. Environ. Prot. Ecol., 19 (2018) 826–836.
[49] N.K. Amin, Removal of direct blue-106 dye from aqueous solution using new activated carbons developed from pomegranate peel: adsorption equilibrium and kinetics., J. Hazard. Mater., 165 (2009) 52–62.
[50] Y. Liu, Some consideration on the Langmuir isotherm equation, Colloids Surf., A, 274 (2006) 34–36.
[51] A.O. Alade, O.S. Amuda, T.J. Afolabi, A.A. Okoya, Adsorption of naphthalene onto activated carbons derived from milk bush kernel shell and flamboyant pod, J. Environ. Chem. Ecotoxicol., 4 (2012) 124–132.
[52] M.M. Kostić, M.D. Radović, J.Z. Mitrović, D.V. Bojić, D.D. Milenković, A.L. Bojić, Application of new biosorbent based on chemicaly modified *Lagenaria vulgaris* shell for the removal of copper(II) from aqueous solutions: effects of operational parameters, Hem. Ind., 67 (2013) 559–567.
[53] D. Dutta, D. Thakur, D. Bahadur, SnO_2 quantum dots decorated silica nanoparticles for fast removal of cationic dye (methylene blue) from wastewater, Chem. Eng. J., 281 (2015) 482–490.

[54] M. Kostić, M. Radović, J. Mitrović, M. Antonijević, D.Bojić, M. Petrović, A. Bojic, Using xanthated *Lagenaria vulgaris* shell biosorbent for removal of Pb(II) ions from wastewater, J. Iran. Chem. Soc., 11(2014) 565–578.
[55] C.B. Vidal, A.L. Barros, C.P. Moura, A.C.A. de Lima, F.S. Dias, L.C.G. Vasconcellos, P.B.A. Fechine, R.F. Nascimento, Adsorption of polycyclic aromatic hydrocarbons from aqueous solutions by modified periodic mesoporous organosilica, J. Colloid Interface Sci., 357 (2011) 466–73.
[56] N. Wang, Y. Zhang, F. Zhu, J. Li, S. Liu, P. Na, Adsorption of soluble oil from water to graphene, Environ. Sci. Pollut. Res., 21 (2014) 6495–6505.
[57] M.I. Temkin, V.M. Pyzhev, Kinetic of ammonia synthesis on promoted iron catalyst, Acta Physiochimica URSS, 12 (1940) 327–356.
[58] A.O. Dada, A.P. Olalekan, A.P. Olatunya, O. Dada, Langmuir, Freundlich, Temkin and Dubinin–Radushkevich isotherms studies of equilibrium sorption of Zn^{2+} unto phosphoric acid modified rice husk, IOSR J. Appl. Chem., 3 (2012) 38–45.
[59] J. Nastaj, A. Przewłocka, M. Rajkowska-Myśliwiec, Biosorption of Ni(II), Pb(II) and Zn(II) on calcium alginate beads: equilibrium, kinetic and mechanism studies, Pol. J. Chem. Technol., 18 (2016) 81–87.
[60] O. Redlich, D.L. Peterson, A useful adsorption isotherm, J. Phys. Chem., 63 (1959) 1024–1026.
[61] S. Chatterjee, D.S. Lee, M.W. Lee, S.H. Woo, Enhanced molar sorption ratio for naphthalene through the impregnation of surfactant into chitosan hydrogel beads, Bioresour. Technol., 101 (2010) 4315–4321.
[62] A.C. Ion, I. Ion, A. Culetu, Adsorption of naphthalene onto carbonic nanomaterial graphitic nanoplatelets in aqueous solutions, UPB Sci. Bull. Ser. B, 73 (2011) 55–66.
[63] S.Y. Lee, S.J. Kim, Adsorption of naphthalene by HDTMA modified kaolinite and halloysite, Appl. Clay Sci., 22 (2002) 55–63.
[64] P. Sivakumar, P.N. Palanisamy, Adsorption studies of Basic Red 29 by a non-conventional activated carbon prepared from *Euphorbia antiquorum* L, Int. J. Chem. Tech. Res., 1 (2009) 502–510.
[65] F.A. Dawodu, K.G. Akpomie, Simultaneous adsorption of Ni(II) and Mn(II) ions from aqueous solution unto a Nigerian kaolinite clay, J. Mater. Res. Technol., 3 (2014) 129–141.
[66] M. Irannajad, H.K. Haghighi, Removal of Co^{2+}, Ni^{2+}, and Pb^{2+} by manganese oxide-coated zeolite: equilibrium, thermodynamics, and kinetics studies, Clays Clay Miner., 65 (2017) 52–62.
[67] M. Kostić, M. Đorđević1, J. Mitrović, N. Velinov, D. Bojić, M. Antonijević, A. Bojić, Removal of cationic pollutants from water by xanthated corn cob: optimization, kinetics, thermodynamics, and prediction of purification process, Environ. Sci. Pollut. Res., 24 (2017) 17790–17804.